Shock Wave/Turbulent Boundary-Layer Interactions with and without Surface Cooling

Lloyd H. Back* and Robert F. Cuffel†
Jet Propulsion Laboratory, California Institute of Technology, Pasadena, Calif.

An experimental investigation was conducted to delineate the structure of the flowfield and temperature distributions in a shock wave/turbulent boundary-layer interaction with and without surface cooling. The Mach number upstream was about 3.5, and the wave angle was 23°. The wall to stagnation temperature ratio was 0.44 with cooling and 1.1 with heating. A detailed map of the interaction flowfields deduced from numerous boundary-layer traversing stations revealed the influence of wall cooling on the flowfield, wave structure, and size of the flow separation region. With surface cooling, the size of the separation region was much smaller, and the separation and reflected shock waves merged together near the edge of the velocity boundary layer, extending into the freestream as one wave. The measured rise in pressure p_2/p_1 across the interactions of 3.1-3.2 could be estimated using oblique shock relations in conjunction with the observation that the mass flux $\rho V \propto 1/r$ in the expanding flow between the incident and separation shock waves in the diffuser. The increase in the measured heat-transfer coefficient $h_2/h_1 = 2.3$ and wall shear stress $\tau_2/\tau_1 = 1.6$-1.7 across the interactions were estimated reasonably well by using semiempirical relations.

Nomenclature

c_p	= specific heat at constant pressure
h	= heat-transfer coefficient
H	= enthalpy or shape factor
M	= Mach number
p	= static pressure
p_t	= stagnation pressure
p_t'	= pitot pressure
q_w	= wall heat flux
r	= radial distance
S_i, S_s, S_r	= incident, separation, and reflected shock waves
T	= temperature
T_t	= stagnation temperature
T_t^+	= dimensionless temperature $(T_t - T_w)/q_w/\rho_w u_\tau c_{p_w})$
u	= velocity component parallel to wall
u^+	= dimensionless velocity u/u_τ
u_τ	= friction velocity $(\tau_w/\rho_w)^{1/2}$
V	= velocity
y	= distance normal to wall
y^+	= dimensionless normal distance $\rho_w u_\tau y/\mu_w$
z	= axial distance
α	= frictional heating parameter $u_\tau^2/2c_{p_w}T_w$
β	= heat-transfer parameter $q_w/T_w \rho_w u_\tau c_{p_w}$
δ	= velocity boundary-layer thickness
δ^*	= displacement thickness
Δ	= thermal boundary-layer thickness
θ	= momentum thickness
λ	= angle between flow and shock wave
μ	= viscosity
ρ	= density
σ	= shock wave flow deflection angle
τ_w	= wall shear stress
ψ	= stream function

Subscripts

1	= upstream of incident shock wave
℄	= centerline
e	= condition at edge of boundary layer
t	= stagnation condition
w	= wall condition

Received June 30, 1975; revision received Sept. 22, 1975. This work presents the results of one phase of research carried out in the Propulsion and Materials Research Section of the Jet Propulsion Laboratory, California Institute of Technology, under Contract NAS7-100, sponsored by NASA.

Index categories: Shock Waves and Detonations; Boundary Layers and Convective Heat Transfer—Turbulent; Nozzle and Channel Flow.

*Member Technical Staff, Propulsion and Materials Research Section. Associate Fellow AIAA.

†Member Technical Staff, Propulsion and Materials Research Section.

Introduction

MANY experimental investigations have been made in the past on the flowfield and heat transfer in shock wave/turbulent boundary-layer interactions, e.g., Refs. 1-13. However, there is little information on the variation of the structure of the flowfield and temperature distributions in interaction regions with the amount of surface cooling.

This investigation was undertaken to determine the mean flowfield and temperature distributions in a shock wave/turbulent boundary-layer interaction along a surface which could be either cooled or heated. The impinging oblique shock wave produced an interaction region in which other waves were formed that contributed, along with the incident wave, to the overall compression of the flow. The flowfield in such an interaction depends upon the upstream Mach number of the external flow, the inclination angle of the impinging shock wave, the mean structure of the boundary layer and its thickness before the interaction, and on surface cooling, as will be seen. In the interactions examined herein (Figs. 1 and 2) the impinging shock wave penetrated deeply into the boundary layer, and, because of the abrupt pressure rise in the flow in the near vicinity of the surface, the momentum deficient shear layer separated, reattached, and underwent subsequent redevelopment downstream of the interactions. Measurements were made with surface cooling which often is necessary to maintain the integrity of surfaces subjected to high-stagnation-temperature streams and on which shock waves may impinge to increase further the heat transfer, e.g., in supersonic diffusers, supersonic inlets of air-breathing engines, and along parts of vehicles in supersonic flight.[14] Measurements also were made with a relatively small amount of surface heating in order to appraise the influence of the thermal boundary condition. The influence of wall cooling on the increase in surface pressure across shock wave/turbulent

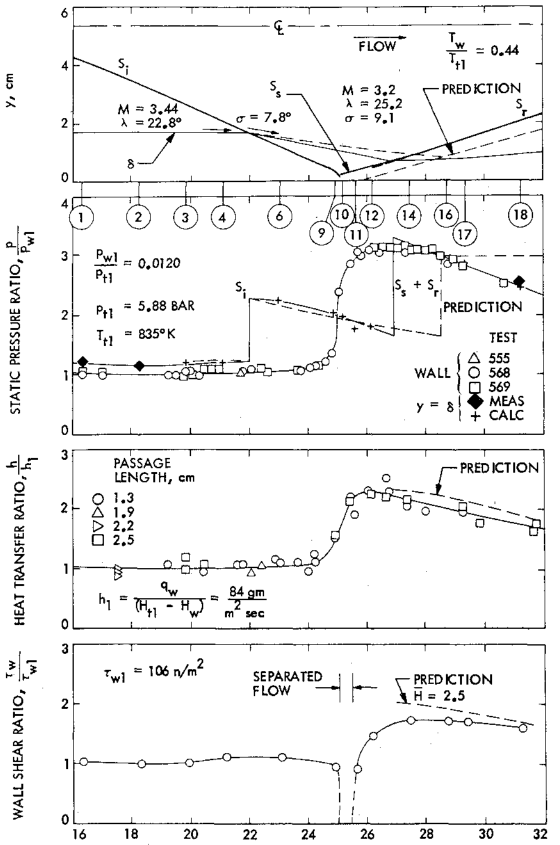

Fig. 1 Shock wave/turbulent boundary-layer interaction with surface cooling.

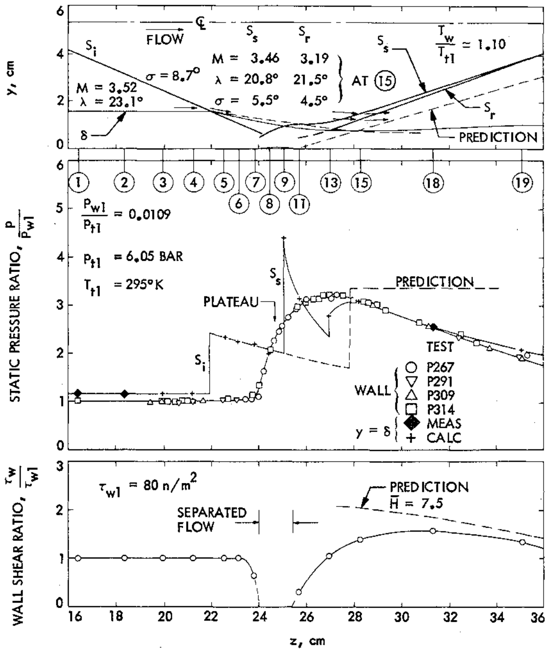

Fig. 2 Shock wave/turbulent boundary-layer interaction with surface heating.

boundary-layer interactions has been found to be relatively small, as indicated by the measurments of Gulbran et al.[8] at high Mach numbers over a range of wall to stagnation temperature ratios T_w/T_t from 0.3 to 0.8. This trend is consistent with the present measurements, although the influence of wall cooling is to change the flow structure and position of the separation shock wave S_s.

Experimental Apparatus and Measurements

The test section consisted of a short subsonic duct 12.7 cm in diameter and 1.4 diam in length, a supersonic conical nozzle with convergent and divergent half-angles of 10° and a circular arc throat with a 4.04-cm-diam throat, and a diffuser with a relatively long second throat of 10.8 cm diam and 11 diam in length. Ambient air was compressed and heated at a remote distance upstream of the subsonic duct by combustion of a small amount of methanol introduced by a spray nozzle. The flow was accelerated in a contraction section (area ratio 11.6), downstream of a calming section, to a nearly uniform flow at the subsonic duct inlet with a fairly thin velocity boundary layer. This boundary layer was turbulent as a result of a boundary-layer trip located just upstream of the subsonic duct inlet, where cooling began. The flow discharged into the atmosphere from the diffuser.

The measurements reported were made in the constant-daimeter region of the diffuser where a shock wave, generated upstream by the compressive turning of the flow in entering the diffuser, impinged on the turbulent boundary layer along the wall. The boundary layer was determined to be turbulent by its structure in the wall region discussed subsequently. The Mach number upstream was about 3.5, and the wave angle was 23°.

By heating the air at the remote distance upstream to $T_{t_l} = 835$°K and by circulating water through individual, circumferential coolant passages, a cooled wall to stagnation temperature ratio T_w/T_{t_l} of 0.44 was obtained. The surface heating condition was achieved by using ambient temperature air ($T_{t_l} = 295$°K) and circulating heated water through the circumferential passages, the temperature ratio T_w/T_{t_l} being 1.1. For both thermal boundary conditions, the upstream stagnation pressure p_{t_l} was about 6 bars. Compression of the air to ambient pressure occurred far downstream of the shock wave/turbulent boundary-layer interaction in a pseudoshock region. Since the flow passed through the choked nozzle preceding the diffuser, the momentum fluxes were nearly the same in the freestream before both interactions. However, because of the different flow stagnation temperatures, the unit Reynolds numbers $\rho_e u_e/\mu_e$ and velocity boundary-layer thickness δ were different before the interactions. For surface cooling, $\rho_e u_e^2 = 1410$kg/(cm-sec^2), $\rho_e/\gamma_e = 8.9\times10^4$ cm^{-1}, and $\delta = 1.65$ cm; and for surface heating, $\rho_e u_e^2 = 1340$ kg/(cm-sec^2), $\rho_e u_e/\mu_e = 3.7\times10^5$ cm^{-1}, and $\delta = 1.52$ cm. To obtain a detailed map of the interactions, boundary-layer measurements were made upstream, within, and downstream of impingement at numerous axial locations (Figs. 1 and 2). These measurements are described subsequently.

The static pressure distribution along the surface was determined from numerous sharp-edge 0.51-cm-diam taps. Differences between the wall static pressure and the ambient pressure were measured with transducers. Stagnation temperature was measured just upstream of the nozzle by three thermocouples spaced 90° apart circumferentially and 2.5 cm from the axis. These thermocouples generally read within 1% of one another. The air mass flow rate was measured with an orifice upstream of the combustor, and, for the hot-flow tests, a rotometer was used to measure the mass flow rate of methanol.

The wall heat flux for each circumferential passage was calculated from the measured water mass flow rate, water temperature difference, and passage gas-side surface area. A correction for the heat loss to the surroundings was made by obtaining measurements with no internal airflow. Most of the 2.5-cm-long passages contained water sidewall thermocouples; when not measured, this temperature was obtained from the average bulk water temperature and the passage heat flux by using conventional heat-transfer relations for channel flow. The gas-side surface temperatures T_w then were calculated from the heat conduction equation.

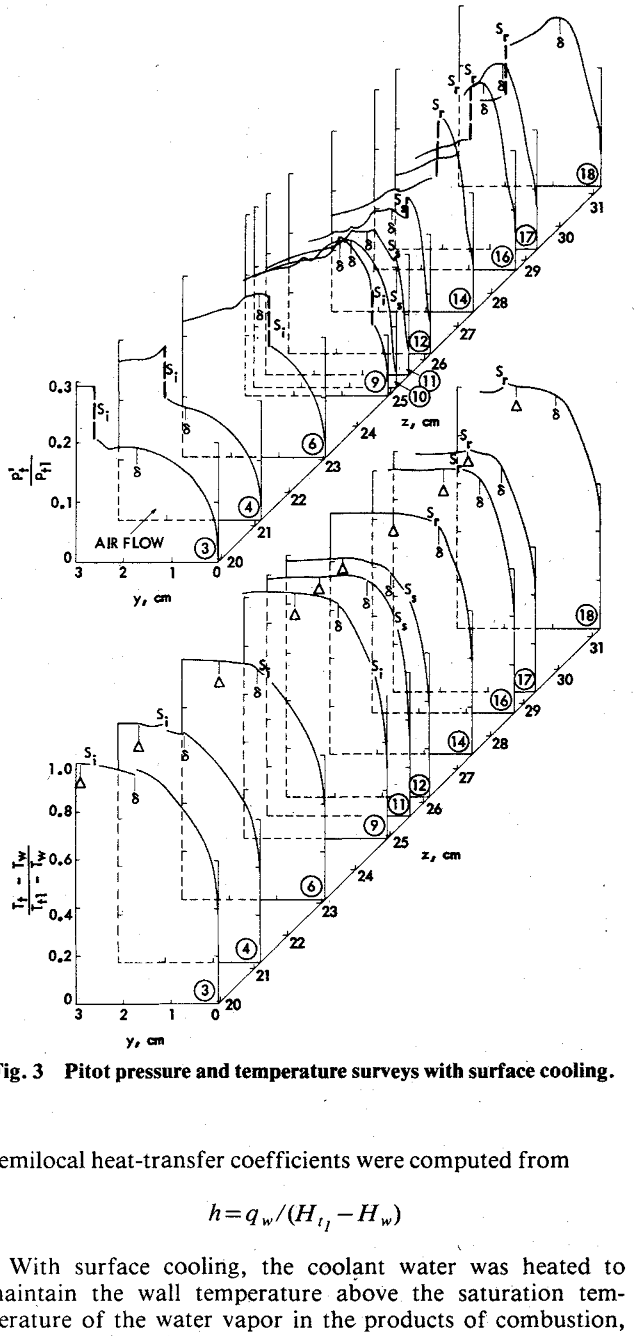

Fig. 3 Pitot pressure and temperature surveys with surface cooling.

Semilocal heat-transfer coefficients were computed from

$$h = q_w / (H_{t_l} - H_w)$$

With surface cooling, the coolant water was heated to maintain the wall temperature above the saturation temperature of the water vapor in the products of combustion, and thus to prevent condensation on the wall. The water flow rate for each passage was measured with a rotometer (near midscale readings), and the temperature difference of water flowing through each passage was measured with three-pair difference thermocouples. The flow rates through the passages were adjusted to maintain nearly the same temperature rise in each passage in order to minimize axial conduction between passages.

The wall shear stress also could be estimated from the boundary-layer measurements obtained with relatively small probes that extended into the viscous sublayer upstream and downstream of the interactions. Semiempirical analyses are considered in conjunction with the measurements in order to obtain additional information about the flow and to determine the change in heat transfer and wall shear stress across the interactions.

Thermodynamic and flow variables were calculated for the products of combustion for the heated-air case, but transport properties were calculated for air,[15] since the methanol-to-air mass flow rate was only 3.1% (see Ref. 16 for the negligible effect of a small amount of water vapor on the viscosity of air). Calculated temperatures of the products of combustion,

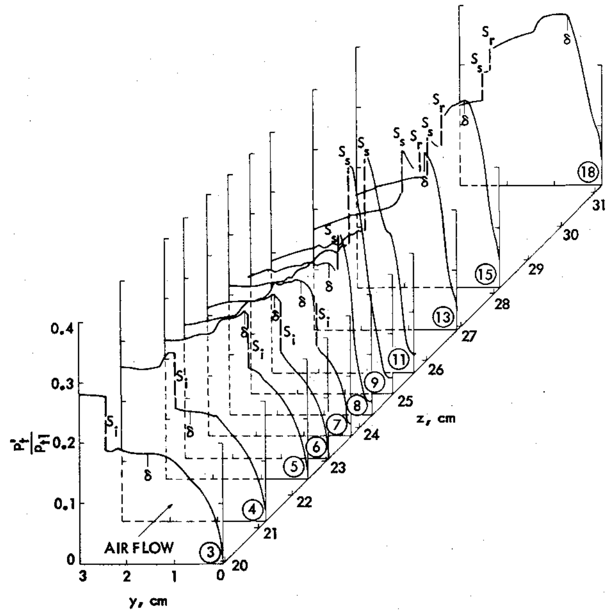

Fig. 4 Pitot pressure surveys with surface heating.

with the assumption of complete chemical reactions, were 1-2% higher than the measured gas temperature.

Probes and Measurements

Boundary-layer surveys were made across the flow with small, flattened pitot tubes 0.010-0.015 cm thick with a 0.005-cm-high opening, and an aspirating thermocouple probe 0.025 cm thick. These probes were similar in construction to those shown in Fig. 2 of Ref. 17, except that the tips were flattened. With the probes resting on the surface, the distances from the center of the probes to the surface were determined by visual observation with a 64-power telescope with a lens scale. The pitot tube was located 45° circumferentially from the temperature probe. These probes were inserted in a ring 3.8 cm long that was moved from one axial location to another from test to test at the same operating condition. In the data reduction, a value of the specific heat ratio $\gamma = 1.4$ was used.

The probes were moved normal to the surface by a micrometer lead screw. The surface location was determined by electrical contact, and the probe location from the surface was determined with a helipot. The probes were motor-driven at speeds up to 0.6 cm/min in the outer part of the boundary layer but were stopped and started to make measurements near the surface. The pressure difference between the pitot tube and wall static pressure tap was measured with a transducer. The output signals of the transducer and thermocouple were plotted vs distance from the surface. The length and diameter of the tubes connecting the pitot tube and wall pressure tap to the differential transducer were chosen to minimize the response of a simultaneous step pressure input at the probe tip and wall tap. At the traversing speeds used in the outer part of the boundary layer, no difference was observed between the readings obtained by traversing away from the surface to the edge of the boundary layer and then back again toward the surface.

Because of the presence of shock waves in the boundary layer, some discussion of the influence of these waves on the probe readings is in order, along with some estimates of the accuracy of the measurements. The pitot tube measurements are believed to be accurate in the vicinity of shock waves, as indicated by the measurements in Ref. 18, where the pitot bow shock/oblique shock wave interaction influenced the pitot tube reading only at distances less than one tip height from the oblique shock wave. A small pitot tube, therefore, also is a good indicator of shock wave position, as shown in Figs. 3

and 4 by the abrupt change in pitot pressure in traversing across shock waves. A more detailed pitot tube traverse across an oblique shock wave was shown in Ref. 19, Fig. 1. From the pitot probe readings on either side of the the oblique shock and the known upstream stagnation pressure, the orientation of the flow to the oblique shock wave is specified. The effect of yaw on the pitot reading is expected to be negligible downstream of the incident wave, which turned the flow, at most, through an 8.5° angle. (Figs. 1 and 2). Pitot tube readings are shown in Figs. 3 and 4 up to the location where the probe was resting on the wall.

Whereas the pitot tube measurements are believed to be reliable, except in separation regions, this was not the case for measurements with a static pressure probe which also was traversed across the flow. This probe had a blunted conical tip, an o.d. of 0.051 cm, and was located 45° circumferentially from the pitot tube in the ring. Static pressure holes, 0.020 cm diam were located on both sides of the probe at a distance either 10 or 15 probe diameters from the tip. This distance has been found to be sufficient to allow the local static pressure to recover to within about 2% of the static pressure upstream of the probe bow shock wave.[20] The present experience, however, has indicated limitations on the use of static pressure probes in the vicinity of shock waves[19] and in the flow inclination region downstream of the incident shock wave, similar to that observed earlier.[21] In the wall vicinity, the readings checked well with the wall pressure tap data. Consequently, the static pressure probe measurements were viewed with caution and were used only in some of the data reduction. For the calculation of the streamlines and velocity distributions, the static pressure was taken to be invariable radially at the wall value (established from wall pressure tap readings) and thus to undergo a step change across shock waves. However, in order to be consistent with a measured 15% rise in static pressure over the outer half of the boundary layer upstream of the interactions, presumably because the flow had passed through an expansion fan further upstream at the entrance of the second throat,[22] the total pressure at the edge of the boundary layer upstream of the interactions was evaluated from the pitot and static pressure measurements. The change in total pressure across the incident shock wave then was calculated using the upstream conditions and the experimentally determined angle between the local flow and the shock wave. From this calculated total pressure and the measured pitot pressures, the local value of the static pressure at the edge of the boundary layer was established between the incident and separation shock waves (Figs. 1 and 2). The measured static pressure was constant across the flow downstream of the interactions, and agreement between these measured values and the calculated values added credence to the procedure used to obtain static pressures between the shock waves. Flow directions thus calculated upstream and downstream of the shock waves (Figs. 1 and 2) also agreed quite well with the streamline orientations discussed subsequently.

The recovery factor for the temperature probe was determined by calibration in the freestream at the traversing stations for the heated-air case. The recovery factor varied from 0.91 to 0.94. These recovery factors were used in reducing the data across the boundary layer, even in the lower Mach number regions nearer the surface, although the errors so introduced were relatively small. In the near vicinity of the surface between the pitot tube and the temperature probe locations, with both probes resting on the wall, the temperature profile was extrapolated toward the wall, guided by the known gas-side wall temperature and the temperature gradient at the wall obtained from the measured wall heat flux. Errors associated with this extrapolation are expected to be small, especially for the velocity distribution, since the velocity depends upon the square root of the static temperature. Since the thermal boundary-layer thickness Δ is greater than the velocity boundary-layer thickness δ (Fig. 3), the measured static pressures were used in the outermost part of the flow, and this led to small step changes in the temperature profiles at δ as a result of the calculation procedure.

Heat-transfer measurements obtained by calorimetry were made with various length circumferential coolant passages as indicated in Fig. 1 for the cooled-surface condition. Unfortunately, it was not possible to obtain reliable heat-transfer measurements for the relatively small amount of surface heating. Local stagnation temperatures also are not reported with surface heating because of the relatively small differences between the thermocouple recovery temperature and the local stagnation temperature. However, since the total temperature change across the boundary layer is small with surface heating, the static temperatures still were known fairly accurately, and, thus, the error in velocity still was expected to be small. Further description of the measurements appears in the discussion of results.

Results

The overall features of the interactions are shown in Fig. 1 for surface cooling and in Fig. 2 for surface heating. The axial locations of the measurement stations are identified by num-

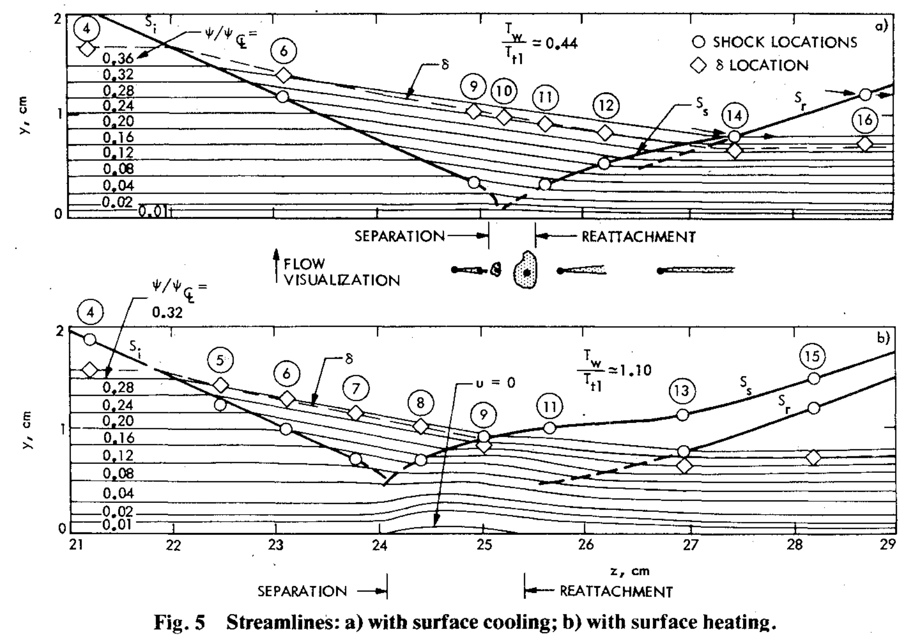

Fig. 5 Streamlines: a) with surface cooling; b) with surface heating.

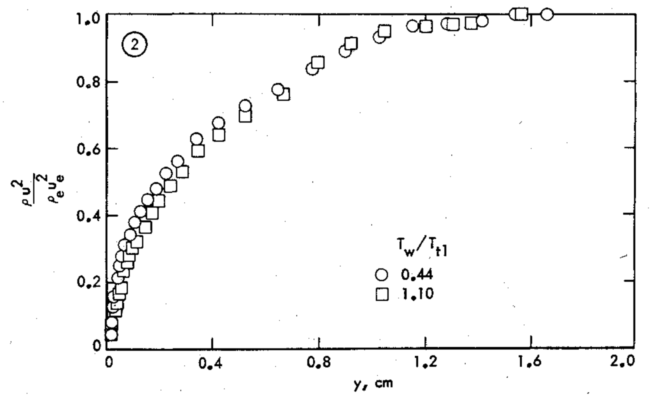

Fig. 6 Momentum flux profiles before the interactions with surface cooling and heating.

bers. The shock wave pictures were constructed from the pitot pressure measurements that are shown in Figs. 3 and 4 for surface cooling and heating, respectively. The vertical dashed lines in Figs. 3 and 4 represent the change in pitot pressure across the shock waves and thus indicate the relative strength of the waves. The waves are indentified as follows: incident shock S_i, separation shock S_s, and reflected shock S_r. The separation shock wave was produced by the coalescing of compressive waves, formed as the flow in the near vicinity of the surface separated upstream of the incident shock wave in the region of the abrupt pressure rise. The other shock wave S_r, extending downstream, was generated by the compressive turning of the flow back again to follow along the surface.

The picture of the flowfield and wave structure is more evident in Figs. 5a and 5b, where streamlines are plotted with surface cooling and surface heating, respectively. The streamlines were obtained from the stream function

$$\psi = \int \rho u r dy$$

and then normalized by the centerline value for the measured flow through the nozzle upstream for each test. Since information is not available on reverse flow velocities in the separation region, the velocity in the reverse flow region was taken as zero, thus making the $u = 0$ line the zero streamline. From velocity gradients observed in the downstream direction with surface heating, the estimated correction for the reverse flow would shift these streamlines toward the centerline by about 0.01 cm. Correction for the variable pressure across the upstream traverses would cause the outermost streamline drawn to shift toward the wall by about 0.01 cm. There really was no way to check the accuracy of the streamline locations near the shock waves, except that it is noted that the flow directions indicated by the streamlines are nearly those deduced from the measurements across the shock waves in the outer part of the flow. With surface cooling, the separation shock S_s and reflected shock S_r merge together sooner than with surface heating. This occurs because the separation region is smaller with surface cooling and thus the separation shock is weaker, only slightly turning the flow. The additional compressive turning required to align the flow with the wall generates the reflected shock wave which reinforces and joins the separation shock near δ with surface cooling. With surface heating, the separation shock does not merge with the reflected shock until well into the freestream. For both interactions, not only is the boundary layer compressed and reduced in thickness, but it looses mass as well, as indicated by the streamlines crossing the boundary-layer thickness between the incident and separation shock waves. The wave pattern indicated is quite different from that observed at lower Mach numbers or in laminar boundary layers (e.g., see Liepmann et al[23]).

It is clear from these observations that the size of the separation region, and therefore the position of the separation shock, was influenced by the thermal boundary condition. The lengths of the separation region were 0.46 and 1.35 cm, and the heights were 0.01 and 0.07 cm, with surface cooling and heating, respectively. This height was estimated from the pitot tube traverses.) In fact, with surface cooling, flow separation could be detected conclusively only by coating the surface with a thin film of ammonia-sensitive Ozalid paint and bleeding a small amount of ammonia gas through the wall static pressure tap holes. The streak patterns obtained from this flow visualization technique are shown in Fig. 5a. The longer separation region with surface heating could be detected by the pitot pressure probe. Separation apparently was delayed with surface cooling because of the somewhat larger momentum fluxes in the boundary layer near the wall, as indicated in Fig. 6. although the freestream Mach number upstream of the interaction was slightly less, too. The upstream influence of the interactions was less than the boundary-layer thickness δ_1 upstream of the interaction, primarily because of the small thickness of the subsonic portion of the boundary layer through which disturbances can travel upstream and be attenuated, i.e., $\delta_1/y_{M=1} = 145$ with surface cooling. The onset of a partial wall static pressure plateau is barely evident in Fig. 2 with surface heating, for which the separation region was larger.

The flow in the outer part of the boundary layer and in the external stream between the incident and separation shock waves accelerates to maintain the mass balance for the flow through the diffuser. The flow also accelerates again down-

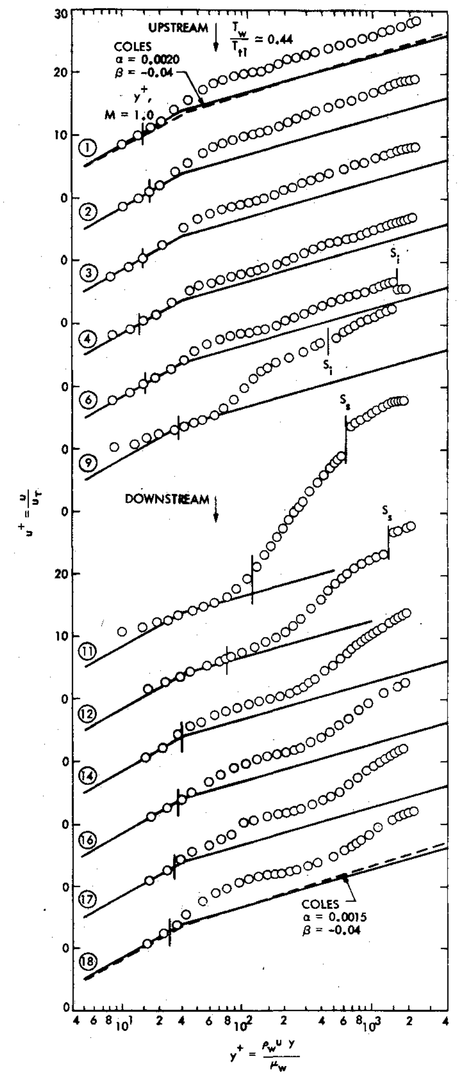

Fig. 7 Velocity distributions upstream and downstream of the interaction with surface cooling.

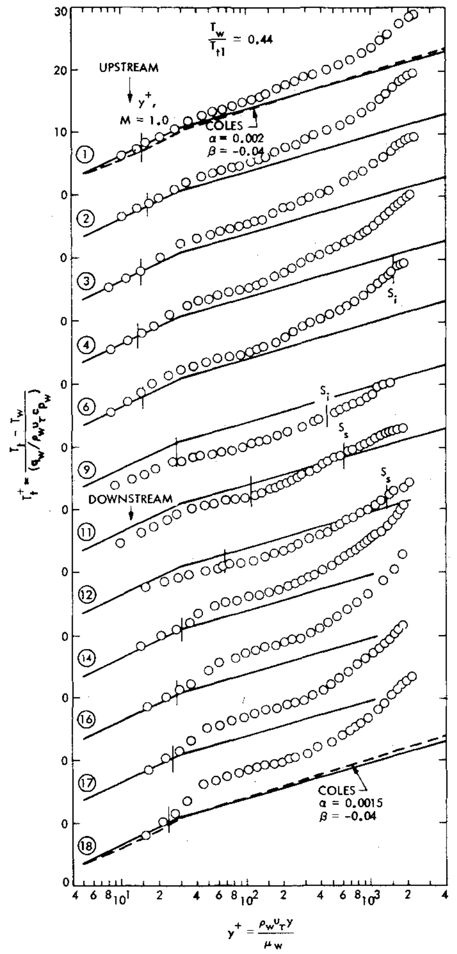

Fig. 8 Temperature distributions upstream and downstream of the interaction with surface cooling.

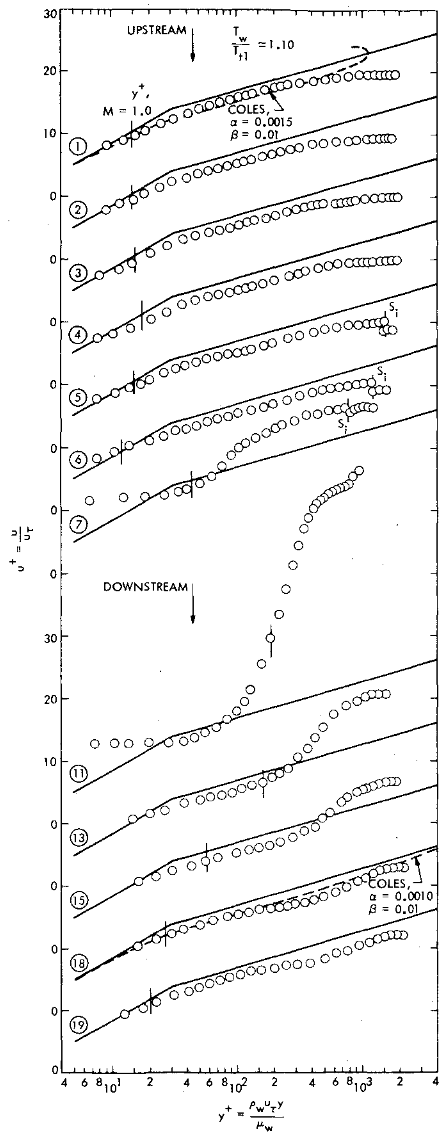

Fig. 9 Velocity distributions upstream and downstream of the interaction with surface heating.

stream of the interactions in the diffuser, as indicated by the wall pressure measurements. In the region between the incident and separation shocks, it was observed that local mass fluxes ρV varied inversely with radius r, since the streamlines are parallel to each other (Figs. 5a and 5b). From this relation, along with the oblique shock wave relations, the pressure rise across the interactions could be predicted by an iterative calculation scheme, the result being shown in the top two graphs of Figs. 1 and 2 (labeled "prediction").

The boundary-layer profiles through the interactions are shown in Figs. 7-9 in terms of u^+, T_t^+, and y^+. The reference profiles from Coles' transformation theory[24] depend upon a heat-transfer parameter β and a viscous heating parameter[25] α (Table 1). For cooling $\beta<0$, and for heating $\beta>0$. With surface heating (Fig. 9), the wall shear stress via the friction velocity $u_\tau = (\tau_w/\rho_w)^{1/2}$ was selected to provide a reasonable fit of the data to the appropriate Coles' profile in the viscous sublayer. With wall cooling, a previous experimental investigation[25,26] has indicated that Coles' transformation theory does not predict adequately the high-speed turbulent boundary layer as also observed herein, so that the von Karman reference curve, shown in Figs. 7 and 9 by the solid line, was used to fit the data in the viscous sublayer. Near separation in the decelerated flow region, the velocity profiles have a large wake component, similar to that observed in low-speed flows in adverse pressure gradient regions, e.g., Ref. 27.

The temperature profiles shown in Fig. 8 indicate that, upstream and downstream of the interaction, the profiles beyond the sublayer lie considerably above the von Karman profile shown as a reference curve. Correspondingly, the thermal resistance is larger (proportional to T_t^+), and, consequently, the von Karman form of Reynolds analogy, as well as other forms such as the Colburn relation, would overestimate the heat transfer.

The change in heat-transfer coefficient across the interaction can be predicted by using a heat-transfer specification known to apply for accelerating and decelerating turbulent boundary layers in conjunction with the integral form of the energy equation.[28] Since the energy defect in the boundary layer is essentially constant because the interaction region is relatively short, and the heat-transfer surface area is consequently small, the change in the heat-transfer coefficient is given by

$$\frac{h}{h_I} = \frac{(\rho_e u_e)}{(\rho_e u_e)_I}\left[\frac{T_e}{T_{e_I}}\right]^{3/4} \tag{1}$$

This estimate agrees reasonably well with the measurements as indicated in the third graph from the top of Fig. 1.

In an analogous way, the change in the wall shear stress across the interaction can be estimated by a specification of a friction relation in conjunction with the use of the integral form of the momentum equation. By using the Blasius relation with a compressibility correction and noting that the interaction region is relatively short and the shear force small, the change in the shear stress is given by

$$\frac{\tau_w}{\tau_{w_I}} = \left[\frac{\rho_e}{\rho_{e_I}}\right]\left[\frac{u_e}{u_{e_I}}\right]^{(1/4)(9+\bar{H})}\left[\frac{T_e}{T_{e_I}}\right]^{3/4} \tag{2}$$

Table 1 Values of β and α with surface cooling and heating

Position	Z, cm	T_w/T_{t_i}	α	β
Surface cooling				
1	16.38	0.429	0.0021	−0.044
2	18.28	0.420	0.0020	−0.044
3	19.91	0.432	0.0021	−0.043
4	21.18	0.447	0.0022	−0.039
6	23.07	0.444	0.0010	−0.041
9	24.92	0.445	0.0010	−0.059
10	25.19	0.424	...	...
11	25.60	0.444	0.0011	−0.053
12	26.18	0.451	0.0017	−0.047
14	27.45	0.438	0.0011	−0.040
16	28.71	0.457	0.0012	−0.036
17	29.34	0.447	0.0013	−0.036
18	31.24	0.435	0.0014	−0.038
Surface heating				
1	16.38	1.125	0.0017	~0.01
2	18.28	1.128	0.0017	~0.01
3	19.91	1.069	0.0017	~0.01
4	21.19	1.094	0.0017	~0.01
5	22.46	1.091	0.0007	~0.01
6	23.09	1.102	0.0008	~0.01
7	23.75	1.095	0.0005	~0.01
8	24.39	1.088	...	...
9	25.02	1.102	...	...
11	25.64	1.107	0.0002	~0.02
13	26.91	1.088	0.0006	~0.01
15	28.19	1.100	0.0008	~0.01
18	31.24	1.103	0.0011	~0.01
19	35.01	1.111	0.0012	~0.01

where $\bar{H}$ is an average shape factor $(\bar{\delta}^*/\bar{\theta})$ across the interaction. Although this estimate does lies somewhat above the values deduced (Figs. 1 and 2), it nevertheless does indicate the magnitude of the change in wall shear stress. With surface cooling, measured values of H were 2.4 and 2.5 upstream and downstream of the interaction, respectively. Corresponding values of H with surface heating were 8.6 and 6.4, respectively, so that the average value of 7.5 was used.

As more appropriate phenomenological turbulence models become available, e.g., Ref. 29, the present set of data should provide a test basis for their evaluation.

References

[1] Vas, I. E., "A Detailed Study of the Interaction of a 14° Shock Wave with a Turbulent Boundary Layer at $M=2.9$," Rept. 296 (AFSOR TN 55-201), April 1955, Princeton Univ., Dept. of Aeronautical Engineering.

[2] Bogdonoff, S. M. and Kepler, C. E., "Separation of a Supersonic Turbulent Boundary Layer," *Journal of Aeronautical Sciences,* Vol. 22, June 1955, pp. 414-424, 430.

[3] Seddon, J., "The Flow Produced by Interaction of a Turbulent Boundary Layer with a Normal Shock Wave of Strength Sufficient to Cause Separation," R and M 3502, March 1960, Ministry of Technology, Aeronautical Research Council, London, Eng.

[4] Sayano, S., Bausch, H. P., and Donnelly, R. J., "Aerodynamic Heating Due to Shock Impingement on a Flat Plate," SM-41331, Aug. 1962, McDonnell-Douglas Aircraft Co., Santa Monica, Calif.

[5] Levin, V. and Fabish, T. J., "Thermal Effects of Shock Wave Turbulent Boundary Layer Interaction at Mach Numbers 3 and 5," 62H-795, Nov. 1962, North American Aviation, Columbus, Ohio.

[6] Pinckney, S. Z., "Data on Effect of Incident-Reflecting Shocks on the Turbulent Boundary Layer," TM X-1221, March 1966, NASA.

[7] Magnan, J. D., Jr. and Spurlin, C. J., "Investigation of Flow Field Interference Caused by Shock Impingement on a Flat Plate at Mach Numbers of 6, 8, and 10," TR-66-85, April 1966, Arnold Engineering Development Center, Arnold Air Force Base, Tenn.

[8] Gulbran, C. E., Redeker, E., Miller, D. S., and Strack, S. L., "Heating in Regions of Interfering Flow Fields, Part III: Two-Dimensional Interaction Caused by Plane Shocks Impinging on Flat Plate Boundary Layers," AFFDL-TR-65-49, Pt. III, March 1967, The Boeing Company, Wright-Patterson Air Force Base, Ohio.

[9] Seebaugh, W. R. and Childs, M. E., "An Experimental Study of the Interaction of a Conical Shock Wave and a Turbulent Boundary Layer Including Suction Effects," AIAA Paper 69-450, June 1969.

[10] Watson, E. C., Murphy, J. D., and Rose, W. C., "Investigation of Laminar and Turbulent Boundary Layers Interacting with Externally Generated Shock Waves," TN D-5512, Nov. 1969, NASA.

[11] Green, J. E., "Reflexion of an Oblique Shock Wave by a Turbulent Boundary Layer," *Journal Fluid Mechanics,* Vol. 40, Pt. 1, Jan. 1970, pp. 81-95.

[12] Alzner, E. and Zakkay, V., "Turbulent Boundary-Layer Shock Interaction with and Without Injection," *AIAA Journal,* Vol. 9, Sept. 1971, pp. 1769-1776.

[13] Holden, M. S., "Shock Wave-Turbulent Boundary Layer Interaction in Hypersonic Flow," AIAA Paper 72-74, Jan. 1972.

[14] Korkegi, R. H., "Survey of Viscous Interactions Associated with High Mach Number Flight," *AIAA Journal,* Vol. 9, May 1971, pp. 771-784.

[15] Hilsenrath, J. et al., "Tables of Thermal Properties of Gases," Circular 564, 1955, National Bureau of Standards, Washington, D.C.

[16] Kestin, J. and Whitelaw, J. H., "The Viscosity of Dry and Humid Air," *International Journal of Heat and Mass Transfer,* Vol. 7, Nov. 1964, pp. 1245-1255.

[17] Back, L. H., Massier, P. F., and Gier, H. L., "Convective Heat Transfer in a Convergent-Divergent Nozzle," *International Journal of Heat and Mass Transfer,* Vol. 7, May 1964, pp. 549-568.

[18] Bannink, W. J. and Nebbeling, C., "Determination of the Position of a Shock Wave from Pitot Tube Experiments," *AIAA Journal,* Vol. 7, April 1969, pp. 796-797.

[19] Back, L. H. and Cuffel, R. F., "Static Pressure Measurements Near an Oblique Shock Wave," *AIAA Journal,* Vol. 9, Feb., 1971, pp. 345-347.

[20] Cronvich, L. L., "Pressure Distributions Over a Cylinder with Conical or Hemispherical Head at Supersonic Velocities," Rept. CM-528, Feb. 1949, Applied Physics Laboratory, Johns Hopkin Univ., Silver Spring, Md., also Shapiro, A.H., *The Dynamics and Thermodynamics of Compressible Fluid Flow,* Vol. II, Ronald Press Co., New York, 1954, pp. 696-697.

[21] Rode, J. E. and Skoglund, V. J.," A Static Pressure Probe for the Interaction Region of a Shock Wave and Boundary Layer," *Journal of Aeronautical Science,* Vol. 29, Oct. 1962, pp. 1262-1263.

[22] Koziak, W. W. and Sullivan, P. A., "Interaction of a Laminar Hypersonic Boundary Layer with a Corner Expansion Wave," *AIAA Journal,* Vol. 11, Aug. 1973, pp. 1057-1058.

[23] Liepmann, H. W., Roshko, A., and Dhawan, S., "On Reflection of Shock Waves from Boundary Layers," Rept. 1100, 1952, NACA.

[24] Coles, D., "The Turbulent Boundary Layer in a Compressible Fluid," *Physics of Fluids,* Vol. 7, Sept. 1964, pp. 1403-1423.

[25] Back, L. H. and Cuffel, R. F., "Turbulent Boundary Layer and Heat Transfer Measurements Along a Convergent-Divergent Nozzle," *Journal of Heat Transfer, Transactions of ASME,* Ser. C, Vol. 93, Nov. 1971, pp. 397-407.

[26] Back, L. H. and Cuffel, R. F., "Turbulent Boundary Layer Measurements Along a Supersonic Nozzle with and Without Wall Cooling," *Journal of Heat Transfer, Transactions of ASME,* Ser. C, Vol. 94, May 1972, pp. 242-243.

[27] Coles, D. E. and Hirst, E. A., *Proceedings—Computation of Turbulent Boundary Layers—1968 AFOSR-IFP-Stanford Conference,* Vol. 2, compiled data, 1968, Sanford Univ., Stanford, Calif.

[28] Back, L. H. and Cuffel, R. F., "Changes in Heat Transfer from Turbulent Boundary Layers Interacting with Shock Waves and Expansion Waves," *AIAA Journal,* Vol. 8, Oct. 1970, pp. 1871-1873.

[29] Wilcox, D. C., "Calculation of Turbulent Boundary-Layer Shock-Wave Interaction," *AIAA Journal,* Vol. 11, Nov. 1973, pp. 1592-1594.